A Waypoint Following Control Design for a Paraglider Model with Aerodynamic Uncertainty

Kazuo Tanaka, *Fellow, IEEE,* Motoyasu Tanaka, *Member, IEEE,* Yutoku Takahashi, and Hua O. Wang, *Senior Member, IEEE*

***Abstract*—This paper presents a waypoint following control design for a powered paraglider (PPG) model. After constructing a dynamic model with six-degree of freedom of the PPG, a dynamical lateral model around a trim equilibrium in the steady-state flight is obtained. Unknown parameters such as the moment of inertia, the drag coefficient, etc., in the lateral model are optimized by real flight experimental data. The model output with the optimized parameters agrees with the real flight experimental data. Since the aerodynamics related parameter, i.e., the drag coefficient, might be slightly changed even near the considered trim equilibrium, this paper considers its uncertainty in the constructed lateral model. A nonlinear controller to stabilize the lateral model (with the aerodynamic uncertainty) on a considered operation domain is designed by solving robust controller design conditions expressed in terms of linear matrix inequality. The experimental results including automatic landing demonstrate the effectiveness of the control system design framework, i.e., the model construction and the robust stable control considering the model uncertainty.**

***Index Terms*—automatic landing, lateral model, powered paraglider, robust control, waypoint following control.**

I. Introduction

In recent years, unmanned aerial vehicles (UAVs) [1]-[3] have become increasingly popular for many applications [4]-[8]. Since the successful pioneer UAV research [1] on helicopter control in the early 90's, UAV control researches have been widely carried out from large-scale UAVs to small-scale UAVs. The recent advances and future development trends for small-scale UAVs were surveyed in [2]. The paper [3] discussed a relation between UAV payload capacities (fixed wing UAVs, rotary wing UAVs, lighter-than-air UAVs) and their endurances, and another relation between UAV performance metric and unit costs. In most of the applications, quadrotors or multirotors, e.g., [9]-[11], have been mainly utilized since their platforms including (semi) autopilot systems with some sensors can be easily purchased in markets. On the other hand, even today, studies on UAVs with fixed wings [12] are not popular in comparison with those on quadrotors since their maintenance, hardware implementation and modeling/control are relatively difficult. Powered paragliders (PPGs) can be considered as unique UAVs that are different from the quadrotors (helicopters) and the other UAVs with fixed wings. However, there are a very few studies on the PPGs in comparison with the quadrotors and the other UAVs with fixed wings.

The existing studies on PPGs presented a motor design [13], a design and manufacturing [14], a radio propagation model construction [15], a project-based learning for educations [16], only simulation studies on path following control [17], [18], and experimental studies only on linear control framework [19]. In our opinion, UAV control studies have to be evaluated through real long-distance (at least kilometers) flight experiments. Even if a designed controller works perfectly only in simulations, the UAV control does not always succeed in real long-distance flight experiments. Some adaptive control schemes on neural networks (NNs), e.g., [20]-[22], have been applied to UAVs. However, these studies have provided only simulation results. In fact, even if adaptive control schemes work perfectly in simulations, they have some difficulties [2] in implementation and/or real flight safety. Even in a few studies dealing with experiments, only specific environments (indoor, no long-distance flight (less than several kilometers), etc.) have been considered. Thus, in real experiments and/or environments, there have been almost no studies on adaptive control of *small-scale* fixed wings and/or PPGs. In this paper, we provide a *nonlinear* control framework for a nonlinear PPG model and show its utility in long-distance flight experiments. In addition, we also succeed in automatic landing control.

To lighten the notation, we will drop the notation with respect to time t before constructing the dynamical lateral model due to providing a number of complicated equations. For instance, we will employ x instead of $x(t)$. After that, we recall the time t notation to clearly show the difference between constant parameters and time-related variables. We also employ the well-known notation for trigonometric functions. In this paper, S_ϕ, C_ϕ and T_ϕ mean $\sin(\phi(t))$, $\cos(\phi(t))$ and $\tan(\phi(t))$, respectively.

II. PPG model construction

Fig. 1 shows an overview of the PPG. Two motors are installed in the PPG. One is a DC motor for controlling the propeller. The other is a servo motor for controlling the direction bar. By tilting the canopy according to the rotation of the direction bar, the PPG can make turns. Fig. 2 shows the system configuration for the autonomous flight control consisting of a gyro, a magnetometer, an accelerometer, a

Manuscript received Sepetember 3, 2014; revised July 10, 2015. This work was supported in part by Grant-in-Aids for Scientific Research (C) 25420215 and (C) 16K00327 from the Ministry of Education, Culture, Sports, Science and Technology of Japan.

K. Tanaka, M. Tanaka and Y. Takahashi are with Department of Mechanical Engineering and Intelligent Systems, The University of Electro-Communications, Tokyo, 182-8585 Japan (email: ktanaka@mce.uec.ac.jp; mtanaka@uec.ac.jp; yutoku.takahashi@rc.mce.uec.ac.jp).

H. O. Wang is with the Department of Mechanical Engineering, Boston University, Boston, MA, 02215, USA (email:wangh@bu.edu).

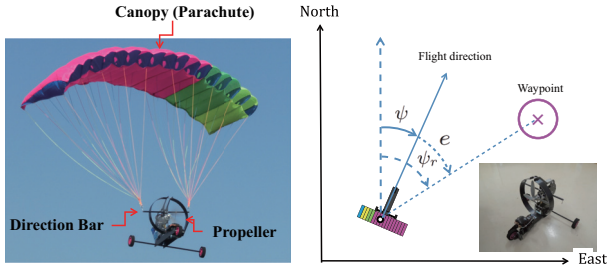

Fig. 1. PPG and variables in waypoint following control.

processor, an electric speed controller, a radio control (RC) receiver unit, a wireless module unit and an on-board camera. The wireless module is used to communicate with the computer on the ground station. With the communication, real PPG flight information (sensors information) is provided in the computer on the ground station. Visual information gathering from the air during flight is separately recorded by the on-board camera. The on-board camera is used to carry out aerial shooting tasks from the air. The wireless module and camera are not used to control the PPG. The sampling rate of the sensors are 10 [Hz]. The control mode (automatic flight control or manual flight control) can be switched by the transmitter on the ground.

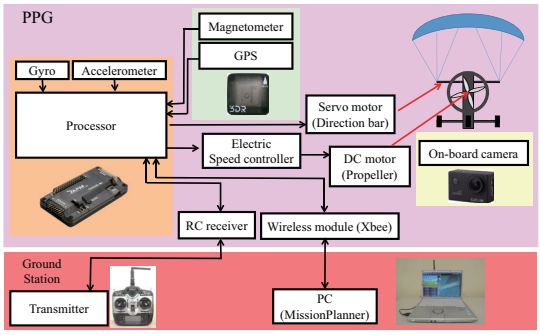

Fig. 2. System configuration.

We consider a PPG model with six degree of freedom on the position (x, y, z) in the world coordinate system and the attitude (ϕ, θ, ψ), i.e., the roll, pitch and yaw angles, around a trim equilibrium. We take a reasonable assumption [23] that the pivot point of the rotational motion is located at the center of the canopy. Table I shows the list of the parameters and variables used in the model construction. This paper utilizes both the inertial frame (fixed to inertial space) and the body frame (fixed to the body). The variables with the subscript 'g' mean those defined in the body frame. In the inertial frame, (x, y, z) axes are defined with the right-handed system, where the x-y plane is set to the horizontal plane, and the positive z-direction is vertically upward. In the body frame, the origin o_g is the center of gravity of the body and (x_g, y_g, z_g) axes are also defined with the right-handed system, where the body heading direction is defined as x_g axis, and the direction from o_g to the canopy center at $\delta = 0$ is defined as z_g axis. From the above definition, the transformation matrix $\boldsymbol{R}$ from the

TABLE I
LIST OF PARAMETERS AND VARIABLES IN MODEL CONSTRUCTION.

x, y, z	positions [m] in inertial frame
ϕ, θ, ψ	roll, pitch, yaw [rad.]
$\boldsymbol{\omega} = [p\ q\ r]^T$	angular velocity vector [rad./s]
V	flight velocity [m/s]
T_H	trust force [N]
δ	direction bar angle [rad.]
I_x, I_y, I_z	moments of inertia of body [kg $\cdot m^2$]
$L = \frac{1}{2}\rho S C_L V^2$	lift force [N]
$D = \frac{1}{2}\rho S C_D V^2$	drag force [N]
C_L, C_D	lift coefficient, drag coefficient
$S = 0.9424$	area of canopy[m^2]
$w = 0.76$	half span of canopy [m]
$d = 0.62$	chord length of canopy [m]
$l = 1.2$	distance between body and canopy center [m]
$m = 1.248$	mass of body [kg]
$g = 9.8$	acceleration of gravity [m/s^2]
ρ=1.2250	air density [kg/m^3]

body frame to the inertial frame can be obtained as

$$\boldsymbol{R} = \begin{bmatrix} C_\theta C_\psi & C_\phi S_\psi + C_\psi S_\phi S_\theta & S_\phi S_\psi - C_\phi C_\psi S_\theta \\ -C_\theta S_\psi & C_\phi C_\psi - S_\phi S_\theta S_\psi & C_\psi S_\phi + C_\phi S_\theta S_\psi \\ S_\theta & -C_\theta S_\phi & C_\phi C_\theta . \end{bmatrix}.$$

In addition, the relation between $\boldsymbol{\omega} = [p\ q\ r]^T$ and the time derivative of ϕ, θ, ψ is given as (1).

$$\begin{bmatrix} \dot{\phi} \\ \dot{\theta} \\ \dot{\psi} \end{bmatrix} = \begin{bmatrix} 1 & S_\phi T_\theta & -C_\phi T_\theta \\ 0 & C_\phi & S_\phi \\ 0 & -S_\phi \sec\theta & C_\phi \sec\theta \end{bmatrix} \begin{bmatrix} p \\ q \\ r \end{bmatrix} \quad (1)$$

The equations of translational and rotational motions in the body frame are represented as

$$\boldsymbol{F}_g = m\frac{d}{dt}\boldsymbol{V}_g + m\boldsymbol{\omega} \times \boldsymbol{V}_g = m \begin{bmatrix} \ddot{x}_g + q\dot{z}_g - r\dot{y}_g \\ \ddot{y}_g + r\dot{x}_g - p\dot{z}_g \\ \ddot{z}_g + p\dot{y}_g - q\dot{x}_g \end{bmatrix}, \quad (2)$$

$$\boldsymbol{M}_g = \frac{d}{dt}\boldsymbol{H} + \boldsymbol{\omega} \times \boldsymbol{H} = \begin{bmatrix} I_x\dot{p} - qr(I_y - I_z) \\ I_y\dot{q} - rp(I_z - I_x) \\ I_z\dot{r} - pq(I_x - I_y) \end{bmatrix}, \quad (3)$$

where $\boldsymbol{V}_g$ denote the velocity vector. The angular momentum $\boldsymbol{H}$ can be replaced with $\boldsymbol{H} = \boldsymbol{I}\boldsymbol{\omega}$, where $\boldsymbol{I}$ denotes the tensor of inertia. $\boldsymbol{I}$ is reasonablely assumed to be a diagonal matrix with zero non-diagonal elements. The assumption is reasonable since it is well-known that the non-diagonal elements (products of inertia) are much smaller than the diagonal elements (moments of inertia). The translational force $\boldsymbol{F}_g$ consists of the following four forces.

$$\boldsymbol{F_g} = \begin{bmatrix} F_{x_g} \\ F_{y_g} \\ F_{z_g} \end{bmatrix} = \begin{bmatrix} T_{H_{x_g}} + L_{x_g} + D_{x_g} + mg_{x_g} \\ T_{H_{y_g}} + L_{y_g} + D_{y_g} + mg_{y_g} \\ T_{H_{z_g}} + L_{z_g} + D_{z_g} + mg_{z_g} \end{bmatrix}, \quad (4)$$

where

$$\begin{bmatrix} T_{H_{x_g}} \\ T_{H_{y_g}} \\ T_{H_{z_g}} \end{bmatrix} = \begin{bmatrix} T_H \\ 0 \\ 0 \end{bmatrix}, \begin{bmatrix} mg_{x_g} \\ mg_{y_g} \\ mg_{z_g} \end{bmatrix} = \boldsymbol{R}^{-1} \begin{bmatrix} 0 \\ 0 \\ -mg \end{bmatrix},$$

$$\begin{bmatrix} L_{x_g} \\ L_{y_g} \\ L_{z_g} \end{bmatrix} = \begin{bmatrix} LS_\theta \\ 0 \\ LC_\theta \end{bmatrix}, \begin{bmatrix} D_{x_g} \\ D_{y_g} \\ D_{z_g} \end{bmatrix} = \boldsymbol{R}^{-1} \begin{bmatrix} -D\dot{x}/V \\ -D\dot{y}/V \\ 0 \end{bmatrix}.$$

The equations of rotational motion (3) is rewritten as

$$\boldsymbol{M}_g = \begin{bmatrix} M_{x_g} \\ M_{y_g} \\ M_{z_g} \end{bmatrix} = \begin{bmatrix} I_x\dot{p} - qr(I_y - I_z) \\ I_y\dot{q} - rp(I_z - I_x) \\ I_z\dot{r} - pq(I_x - I_y) \end{bmatrix}. \quad (5)$$

Considering the viscous resistances $b_{D\phi}$ and $b_{D\theta}$ on x_g and y_g axes, respectively, the rotational force $\boldsymbol{M}_g$ is obtained as

$$\boldsymbol{M}_g = \begin{bmatrix} M_{x_g} \\ M_{y_g} \\ M_{z_g} \end{bmatrix} = \begin{bmatrix} -mg_{y_g}l - b_{D\phi}pl^2 \\ T_H l + mg_{z_g}l - b_{D\theta}ql^2 \\ M_{z_g} \end{bmatrix}, \quad (6)$$

where $M_{z_g} = \rho C_D w\Big(-SVrw + ld(V^2 + r^2w^2)k\delta\Big)$. By applying the transformation matrix $\boldsymbol{R}$ and (1) to (2) and (3), we finally have a PPG model with six degree of freedom in the inertial frame. By considering a trim equilibrium, a longitudinal model and a lateral model can be separately converted from the PPG model with six-degree of freedom. Since this paper focuses on the waypoint following control, we consider only a lateral model. By introducing the trim equilibrium, i.e., $\theta_{trim} = 18[deg.]$ and $V_{trim} = 6.4[m/s]$, we construct a lateral model, where these values are verified using the flight experimental data. The lateral model of the PPG model around the trim equilibrium is described as

$$\begin{aligned} \ddot{x}(t) =& \dot{\psi}(t)\dot{y}(t)C^2_{\theta_{trim}} \\ & - \frac{D(t)\dot{x}(t) - T_H(t)V_{trim}C_{\theta_{trim}}C_\psi(t)}{mV_{trim}}, \quad (7) \\ \ddot{y}(t) =& - \frac{D(t)\dot{y}(t) + T_H(t)V_{trim}C_{\theta_{trim}}S_\psi(t)}{mV_{trim}} \\ & - \dot{\psi}(t)\dot{x}(t)C^2_{\theta_{trim}}, \quad (8) \\ \ddot{\psi}(t) =& \frac{C_D\rho w}{I_z C_{\theta_{trim}}}\{-SV_{trim}wC_{\theta_{trim}}\dot{\psi}(t) \\ & + ld(V^2_{trim}(t) + \dot{\psi}^2(t)w^2C_{\theta_{trim}})k\delta(t)\}. \quad (9) \end{aligned}$$

Since the waypoint following is realized by controlling the PPG heading to the direction of a desired waypoint, we consider the equation (9) with respect to the yaw angle. In (9), the unknown parameters are C_D, I_z, k, where k denotes the coefficient with respect to the input. It is known that airplanes with propellers connected to motors or engines have different sensitivity for left and right turns due to the anti-torque of motors or engines. In our PPG, the propeller turns right, so that the sensitivity of turning left is larger than that of turning right. To represent the anti-torque phenomenon, we set different values as k for the right turn k_r and the left turn k_l. The least squares fitting is carried out to determine these unknown parameters using flight experimental data. The unknown parameters are determined as follows: $C_D = 0.1356$, $I_z = 0.2$, $k_r = 0.3$ and $k_l = 0.7$. The result $k_r < k_l$ reflects the anti-torque property.

Fig. 3 shows the prediction result (10 step ahead prediction) by the PPG model with the identified parameters, where the mean absolute error is 3.983 [deg.]. The model accuracy is reasonable to design a stable controller. However, the model is not perfect. We will design a robust controller by assuming a parameter uncertainty in Section III. Altitude control based on the longitudinal model of the PPG model has reported in [24], [25]. Although the designed controller worked well even in experiments, its direction was controlled by a human operator. In this paper, with respect to altitude control, we utilize the controller designed in [24], [25] and focus on the waypoint following control design for the PPG model. Hence, from now, we will treat only the yaw angle dynamics in the lateral model.

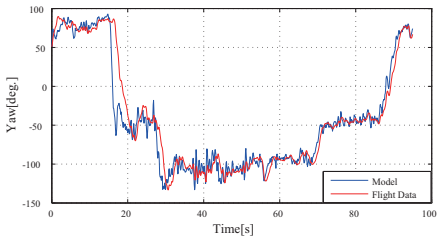

Fig. 3. Prediction result (10 step ahead prediction) (blue line:model output, red line:flight experimental data).

III. Stable Controller Design

Fig. 1 shows also the variables in the waypoint following control, where $\psi(t)$ and $\psi_r(t)$ denote the yaw angle and the desired yaw angle from the north direction Define the yaw angle difference as $e(t) = \psi(t) - \psi_r(t)$. Then, with $e(t)$, (9) can be rewritten as the following error dynamics

$$\begin{aligned} \ddot{e}(t) =& \frac{C_D\rho w}{I_r C_{\theta_{trim}}}\{-SV_{trim}wC_{\theta_{trim}}\dot{e}(t) \\ & + ld(V^2_{trim} + \dot{\psi}^2(t)w^2C_{\theta_{trim}})k\delta(t)\}. \quad (10) \end{aligned}$$

We note that the control purpose is to achieve $e(t) \to 0$. Now we assume that $0 \le |\dot{\psi}(t)| \le v_\psi$. From the real flight experimental data, the upper bound v_ψ is set to a sufficient large value satisfying the assumption, i.e., $v_\psi = \pi/2$. Recall the important property with respect to k, i.e., $k = k_r$ and $k = k_l$ when $\dot{\psi}(t) > 0$ and $\dot{\psi}(t) \le 0$, respectively. In addition, considering an uncertainty for C_D, that is, replacing C_D with $C_D(1 + \Delta C_D(t))$, we have the following model (11), where $||\boldsymbol{\Delta}_{ai}(t)|| \le \frac{1}{\gamma_a}$ and $||\boldsymbol{\Delta}_{bi}(t)|| \le \frac{1}{\gamma_b}$. Note that (11) with $\Delta C_D(t) = 0$, i.e., the nominal system of (11), is equivalent to (10) under $k = k_r$ or $k = k_l$. A robust controller accepting $\pm 20\%$ parameter change from the nominal C_D will be designed later.

$$\begin{aligned} \dot{\boldsymbol{e}}(t) =& \sum_{i=1}^{r}\lambda_i(\dot{e}(t))\{(\boldsymbol{A}_i + \boldsymbol{D}_{ai}\boldsymbol{\Delta}_{ai}(t)\boldsymbol{E}_{ai})\boldsymbol{e}(t) \\ & + (\boldsymbol{B}_i + \boldsymbol{D}_{bi}\boldsymbol{\Delta}_{bi}(t)\boldsymbol{E}_{bi})\delta(t)\}, \quad (11) \end{aligned}$$

where $r = 4$ and $\boldsymbol{e}(t) = [e(t)\ \dot{e}(t)]^T$,

$$\boldsymbol{A}_i = \begin{bmatrix} 0 & 1 \\ 0 & -\frac{C_D\rho w^2}{I_z}SV_{trim} \end{bmatrix}, \boldsymbol{D}_{ai} = \begin{bmatrix} 0 & 0 \\ 0 & 1 \end{bmatrix},$$

$$\boldsymbol{E}_{ai} = \begin{bmatrix} 0 & 1 \\ 0 & -\frac{C_D\rho w^2}{I_z}SV_{trim} \end{bmatrix},$$

$$\boldsymbol{B}_\eta = \begin{bmatrix} 0 \\ \frac{ldV^2_{trim}C_D\rho w k_\eta}{I_z C_{\theta_{trim}}} \end{bmatrix},\ \eta = 1, 2,$$

$$\boldsymbol{B}_\xi = \begin{bmatrix} 0 \\ \frac{ld(V_{trim}^2+v_\psi^2 w^2 C_{\theta_{trim}})C_D\rho w k_\xi}{I_z C_{\theta_{trim}}} \end{bmatrix},\ \xi = 3,4,$$

$$\boldsymbol{D}_{bi} = \begin{bmatrix} 0 & 0 \\ 0 & 1 \end{bmatrix}, \boldsymbol{E}_{b\eta} = \begin{bmatrix} 0 \\ \frac{ldV_{trim}^2 C_D\rho w k_\eta}{I_z C_{\theta_{trim}}} \end{bmatrix},\ \eta = 1,2$$

$$\boldsymbol{E}_{b\xi} = \begin{bmatrix} 0 \\ \frac{ld(V_{trim}^2+v_\psi^2 w^2 C_{\theta_{trim}})C_D\rho w k_\xi}{I_z C_{\theta_{trim}}} \end{bmatrix},\ \xi = 3,4,$$

for $i = 1, \cdots, r$, $k_1 = k_3 = k_r$, and $k_2 = k_4 = k_l$. The λ_i's are defined as $(\lambda_1(\dot{e}(t)), \lambda_2(\dot{e}(t)), \lambda_3(\dot{e}(t)), \lambda_4(\dot{e}(t))) = (\{v_\psi^2 - \dot{e}^2(t)\}/v_\psi^2, 0, \dot{e}^2(t)/v_\psi^2, 0)$ when $\dot{e}(t) \geq 0$, where $v_\psi = \pi/2$. Otherwise, $(0, \{v_\psi^2 - \dot{e}^2(t)\}/v_\psi^2, 0, \dot{e}^2(t)/v_\psi^2)$ when $\dot{e}(t) < 0$. The upper bounds γ_a and γ_b of the uncertainty matrices are set to 5 since $|\Delta C_D(t)| < 0.2$. Note that $\lambda_i(\dot{e}(t)) \geq 0$ and $\sum_{i=1}^r \lambda_i(\dot{e}(t)) = 1$ for all t. The property on λ_i will play an important role in the derivation of stabilization conditions.

Now we construct a controller (12) to stabilize (11).

$$\delta(t) = -\sum_{i=1}^{r} \lambda_i(\dot{e}(t)) \boldsymbol{F}_i \boldsymbol{e}(t) \tag{12}$$

By substituting the controller (12) into (11), we have

$$\dot{\boldsymbol{e}}(t) = \sum_{i=1}^{r}\sum_{j=1}^{r} \lambda_i(\dot{e}(t))\lambda_j(\dot{e}(t))\{\boldsymbol{A}_i - \boldsymbol{B}_i\boldsymbol{F}_j + \boldsymbol{\Omega}_{ij}\}\boldsymbol{e}(t),$$

where

$$\boldsymbol{\Omega}_{ij} = \begin{bmatrix} \boldsymbol{D}_{ai} & \boldsymbol{D}_{bi} \end{bmatrix} \begin{bmatrix} \boldsymbol{\Delta}_{ai} & \boldsymbol{0} \\ \boldsymbol{0} & \boldsymbol{\Delta}_{bi} \end{bmatrix} \begin{bmatrix} \boldsymbol{E}_{ai} \\ -\boldsymbol{E}_{bi}\boldsymbol{F}_j \end{bmatrix}. \tag{13}$$

Consider a candidate of Lyapunov functions $\boldsymbol{e}^T(t)\boldsymbol{P}\boldsymbol{e}(t)$, where $\boldsymbol{P} > \boldsymbol{0}$. Then,

$$\frac{d}{dt}\boldsymbol{e}^T(t)\boldsymbol{P}\boldsymbol{e}(t) = \sum_{i=1}^{r} \lambda_i^2(\dot{e}(t))\boldsymbol{e}^T(t)\boldsymbol{L}_{ii}\boldsymbol{e}(t)$$
$$+\sum_{i=1}^{r}\sum_{i<j} \lambda_i(\dot{e}(t))\lambda_j(\dot{e}(t))\boldsymbol{e}^T(t)\{\boldsymbol{L}_{ij} + \boldsymbol{L}_{ji}\}\boldsymbol{e}(t),$$

where

$$\boldsymbol{L}_{ij} = \boldsymbol{G}_{ij} + \boldsymbol{P}\begin{bmatrix} \boldsymbol{D}_{ai} & \boldsymbol{D}_{bi} \end{bmatrix}\begin{bmatrix} \boldsymbol{D}_{ai}^T \\ \boldsymbol{D}_{bi}^T \end{bmatrix}\boldsymbol{P} + \boldsymbol{\Lambda}_{ij}^T\boldsymbol{\Lambda}_{ij} - \boldsymbol{\Gamma}_{ij}^T\boldsymbol{\Gamma}_{ij},$$

$$\boldsymbol{G}_{ij} = (\boldsymbol{A}_i - \boldsymbol{B}_i\boldsymbol{F}_j)^T\boldsymbol{P} + \boldsymbol{P}(\boldsymbol{A}_i - \boldsymbol{B}_i\boldsymbol{F}_j),$$

$$\boldsymbol{\Lambda}_{ij} = \begin{bmatrix} \boldsymbol{\Delta}_{ai} & \boldsymbol{0} \\ \boldsymbol{0} & \boldsymbol{\Delta}_{bi} \end{bmatrix}\begin{bmatrix} \boldsymbol{E}_{ai} \\ -\boldsymbol{E}_{bi}\boldsymbol{F}_j \end{bmatrix}, \boldsymbol{\Gamma}_{ij} = \begin{bmatrix} \boldsymbol{D}_{ai}^T \\ \boldsymbol{D}_{bi}^T \end{bmatrix}\boldsymbol{P} - \boldsymbol{\Lambda}_{ij}.$$

Note that $\boldsymbol{\Gamma}_{ij}^T\boldsymbol{\Gamma}_{ij} \geq \boldsymbol{0}$ and $\boldsymbol{\Lambda}_{ij}^T\boldsymbol{\Lambda}_{ij} \leq \boldsymbol{\Pi}_{ij}$, where

$$\boldsymbol{\Pi}_{ij} = \begin{bmatrix} \boldsymbol{E}_{ai} \\ -\boldsymbol{E}_{bi}\boldsymbol{F}_j \end{bmatrix}^T \begin{bmatrix} \frac{1}{\gamma_{ai}^2}\boldsymbol{I} & \boldsymbol{0} \\ \boldsymbol{0} & \frac{1}{\gamma_{bi}^2}\boldsymbol{I} \end{bmatrix} \begin{bmatrix} \boldsymbol{E}_{ai} \\ -\boldsymbol{E}_{bi}\boldsymbol{F}_j \end{bmatrix}$$

for all i and j. Therefore, from the property of λ_i, if

$$\boldsymbol{\zeta}_{ii} < \boldsymbol{0},\ \boldsymbol{\zeta}_{ij} + \boldsymbol{\zeta}_{ji} < \boldsymbol{0}, \tag{14}$$

where $\boldsymbol{\zeta}_{ij} = \boldsymbol{G}_{ij} + \boldsymbol{P}\begin{bmatrix} \boldsymbol{D}_{ai} & \boldsymbol{D}_{bi} \end{bmatrix}\begin{bmatrix} \boldsymbol{D}_{ai}^T \\ \boldsymbol{D}_{bi}^T \end{bmatrix}\boldsymbol{P} + \boldsymbol{\Pi}_{ij}$, then $\frac{d}{dt}\boldsymbol{e}^T(t)\boldsymbol{P}\boldsymbol{e}(t) < \boldsymbol{0}$ at $\boldsymbol{e}(t) \neq \boldsymbol{0}$. By Schur complement, the first and second inequalities in (14) are rewritten as (15) and (16), respectively. Therefore, the system (11) with the uncertainty is stabilized via the controller (12) if there exist a common positive definite matrix $\boldsymbol{P}$ and feedback gains $\boldsymbol{F}_i$ satisfying

$$\boldsymbol{S}_{ii} = \begin{bmatrix} \boldsymbol{G}_{ii} & \boldsymbol{\Psi}_{ii} \\ \boldsymbol{\Psi}_{ii}^T & \boldsymbol{\Xi}_{ii} \end{bmatrix} < \boldsymbol{0}, \qquad \forall i, \tag{15}$$

$$\boldsymbol{T}_{ij} = \begin{bmatrix} \boldsymbol{G}_{ij} + \boldsymbol{G}_{ji} & \boldsymbol{\Upsilon}_{ij} \\ \boldsymbol{\Upsilon}_{ij}^T & \boldsymbol{\Phi}_{ij} \end{bmatrix} < \boldsymbol{0}, \quad i < j, \tag{16}$$

where

$$\boldsymbol{\Psi}_{ii} = \begin{bmatrix} \boldsymbol{P}\boldsymbol{D}_{ai} & \boldsymbol{P}\boldsymbol{D}_{bi} & \boldsymbol{E}_{ai}^T & -(\boldsymbol{E}_{bi}\boldsymbol{F}_i)^T \end{bmatrix},$$
$$\boldsymbol{\Upsilon}_{ij} = \begin{bmatrix} \boldsymbol{P}\boldsymbol{D}_{ai} & \boldsymbol{P}\boldsymbol{D}_{bi} & \boldsymbol{P}\boldsymbol{D}_{aj} & \boldsymbol{P}\boldsymbol{D}_{bj} \\ \boldsymbol{E}_{ai}^T & -(\boldsymbol{E}_{bi}\boldsymbol{F}_j)^T & \boldsymbol{E}_{aj}^T & -(\boldsymbol{E}_{bj}\boldsymbol{F}_i)^T \end{bmatrix},$$
$$\boldsymbol{\Xi}_{ii} = block-diag\begin{bmatrix} -\boldsymbol{I} & -\boldsymbol{I} & -\gamma_{ai}^2\boldsymbol{I} & -\gamma_{bi}^2\boldsymbol{I} \end{bmatrix},$$
$$\boldsymbol{\Phi}_{ij} = block-diag\begin{bmatrix} -\boldsymbol{I} & -\boldsymbol{I} & -\boldsymbol{I} & -\boldsymbol{I} & -\gamma_{ai}^2\boldsymbol{I} & -\gamma_{bi}^2\boldsymbol{I} & -\gamma_{aj}^2\boldsymbol{I} & -\gamma_{bj}^2\boldsymbol{I} \end{bmatrix}.$$

The above conditions are not still LMIs. Hence, we convert the above conditions into LMIs by introducing the following variable transformations.

$$\hat{\boldsymbol{S}}_{ii} = \begin{bmatrix} \boldsymbol{H}_{ii} & \hat{\boldsymbol{\Psi}}_{ii} \\ \hat{\boldsymbol{\Psi}}_{ii}^T & \boldsymbol{\Xi}_{ii} \end{bmatrix}, \hat{\boldsymbol{T}}_{ij} = \begin{bmatrix} \boldsymbol{H}_{ij} + \boldsymbol{H}_{ji} & \hat{\boldsymbol{\Upsilon}}_{ij} \\ \hat{\boldsymbol{\Upsilon}}_{ij}^T & \boldsymbol{\Phi}_{ij} \end{bmatrix},$$

where $\boldsymbol{L}_1\boldsymbol{S}_{ii}\boldsymbol{L}_1 = \hat{\boldsymbol{S}}_{ii}$ and $\boldsymbol{L}_2\boldsymbol{T}_{ij}\boldsymbol{L}_2 = \hat{\boldsymbol{T}}_{ij}$,

$$\boldsymbol{L}_1 = block-diag\begin{bmatrix} \boldsymbol{X} & \boldsymbol{I} & \boldsymbol{I} & \boldsymbol{I} & \boldsymbol{I} \end{bmatrix},$$
$$\boldsymbol{L}_2 = block-diag\begin{bmatrix} \boldsymbol{X} & \boldsymbol{I} & \boldsymbol{I} & \boldsymbol{I} & \boldsymbol{I} & \boldsymbol{I} & \boldsymbol{I} & \boldsymbol{I} & \boldsymbol{I} \end{bmatrix},$$
$$\boldsymbol{H}_{ij} = \boldsymbol{X}\boldsymbol{G}_{ij}\boldsymbol{X} = \boldsymbol{X}\boldsymbol{A}_i^T + \boldsymbol{A}_i\boldsymbol{X} - \boldsymbol{B}_i\boldsymbol{M}_j - \boldsymbol{M}_j^T\boldsymbol{B}_i^T,$$
$$\boldsymbol{X} = \boldsymbol{P}^{-1}, \qquad \boldsymbol{M}_i = \boldsymbol{F}_i\boldsymbol{P}^{-1},$$
$$\hat{\boldsymbol{\Psi}}_{ii} = \begin{bmatrix} \boldsymbol{D}_{ai} & \boldsymbol{D}_{bi} & \boldsymbol{X}\boldsymbol{E}_{ai}^T & -(\boldsymbol{E}_{bi}\boldsymbol{M}_i)^T \end{bmatrix},$$
$$\hat{\boldsymbol{\Upsilon}}_{ij} = \begin{bmatrix} \boldsymbol{D}_{ai} & \boldsymbol{D}_{bi} & \boldsymbol{D}_{aj} & \boldsymbol{D}_{bj} \\ \boldsymbol{X}\boldsymbol{E}_{ai}^T & -(\boldsymbol{E}_{bi}\boldsymbol{M}_j)^T & \boldsymbol{X}\boldsymbol{E}_{aj}^T & -(\boldsymbol{E}_{bj}\boldsymbol{M}_i)^T \end{bmatrix},$$

for all i and j. As a result, we arrive at the following LMI stabilization conditions. The feedback gains $\boldsymbol{F}_i$ that stabilize the system (11) with the uncertainty can be obtained by solving the following LMIs: $\boldsymbol{X} > \boldsymbol{0}$, $\hat{\boldsymbol{S}}_{ii} < \boldsymbol{0}$ $(\forall i)$ and $\hat{\boldsymbol{T}}_{ij} < \boldsymbol{0}$ $(i < j)$. The feedback gains can be obtained as $\boldsymbol{F}_i = \boldsymbol{M}_i\boldsymbol{X}^{-1}$ from the solutions $\boldsymbol{X}$ and $\boldsymbol{M}_i$ of the above LMIs.

IV. Control Experiment

A triangle path flight (Experiment I) and a square path flight (Experiment II) are performed in the experiments, where Experiment II contains also automatic landing control to the runway at the end of the square path flight. The altitudes are automatically controlled by using the controller in [24], [25]. In the experiments, take-off of the PPG is manually controlled by operators. Figs. 4 and 5 show the waypoint following control result in Experiment I, where the green circles and the red line in Fig. 4 denote the waypoints (WP1∼WP3) and the flight path, respectively. The 'Starting point' denotes the point of starting the automatic control. The switching to the next waypoint is carried out as soon as the PPG arrives at a

switching circle defined around the waypoint. The center of the switching circle is the waypoint and its radius is 10 [m]. It can be found that the PPG stably flies to the waypoints directly, that is, the designed controller works well. Fig. 5 shows the yaw angle errors in Experiment I. The mean absolute errors (MAEs) during the steady flights are 2.82 [deg.], 6.24 [deg.] and 3.91 [deg.] in the WP1 flight, the WP2 flight and the WP3 flight, respectively. The MAE in the WP2 flight is relatively larger than the other MAEs although it is still sufficient small in the sense of long-distance flight control. The flight path from WP1 to WP2 is the direction against the wind (the WSW direction wind). It is known that some oscillations of UAVs occur during the flight against the wind. Conversely, the controller works well even for the flight against the wind. Fig 6 shows the waypoint following control result in Experiment II, where the altitude is controlled at 40 [m] from the sea level. The four waypoints (WP1∼WP4) are set as a square path flight. In Experiment II also, the PPG stably flies to the waypoints directly. In Fig 6, a set of plural waypoints (WP5∼WP8) on the runway are for the automatic landing control. The WP9 is set to the level of runway. Since the PPG touched down on the runway before arriving at WP9, WP9 is omitted in Fig 6. Fig. 7 shows the control result of the automatic landing and its photos. The potions (1)∼(4) in the upper figure correspond to those of the photos (1)∼(4) in the lower figure, respectively. By monotonically decreasing the target altitude in the plural waypoints set on the runway, we succeed in realizing the landing control.

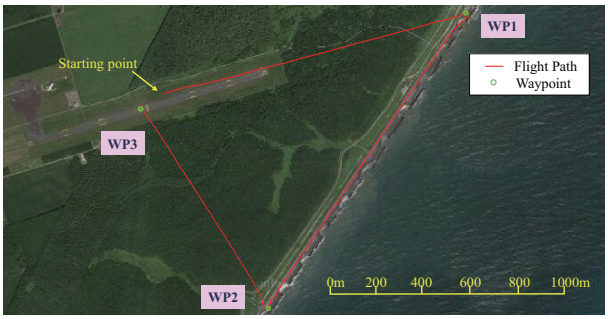

Fig. 4. Control result in Experiment I (Red line:flight path, Green circles:waypoints).

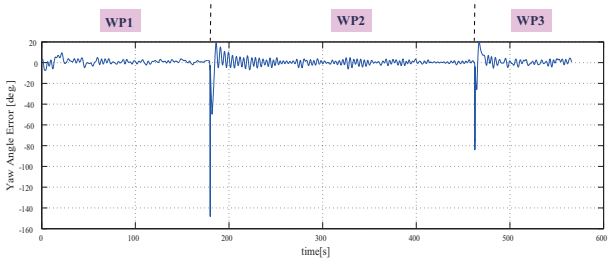

Fig. 5. Yaw angle error in Experiment I.

V. Conclusion

This paper has presented a waypoint following control design for a PPG model. A dynamical lateral model around a trim equilibrium in the steady-state flight has been obtained. Unknown parameters such as the moment of inertia, the drag coefficient, etc., in the lateral model have been optimized by real flight experimental data. A nonlinear controller to stabilize the lateral model with the aerodynamic uncertainty has been designed by solving the LMI robust controller design conditions. The experimental results including automatic landing have demonstrated the effectiveness of the control system design framework. Our next subjects are to realize wind disturbance rejection and some advanced flight tasks.

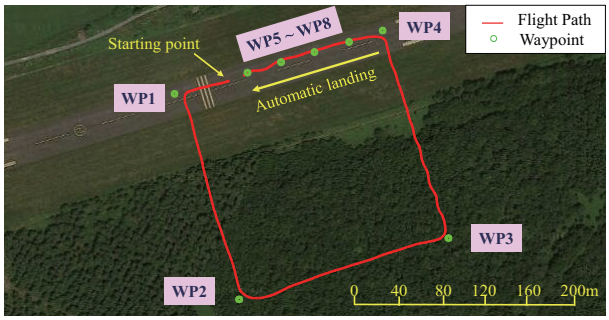

Fig. 6. Control result in Experiment II (Red line:flight path, Green circles:waypoints).

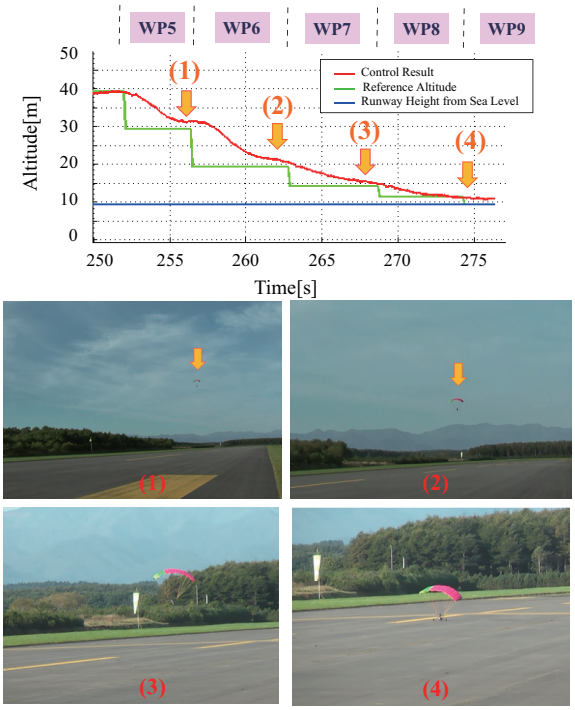

Fig. 7. Automatic landing control result (upper:altitude control result for the set of plural waypoints, lower:photos at the potions (1), (2) (3) and (4)).

References

[1] M. Sugeno, et al., "Fuzzy hierarchical control of an unmanned helicopter," Proceeding of 5th IFSA Congress, Seoul, July 1993, pp.179-182.
[2] G. Cai, J. Dias and L. Seneviratne, "A Survey of Small-Scale Unmanned Aerial Vehicles: Recent Advances and Future Development Trends," Unmanned Systems, Vol.2, No.2, pp.1-25, April 2014.

[3] S. Recoskie, A. Fahim, W. Gueaieb and E. Lanteigne, "Hybrid Power Plant Design for a Long-Range Dirigible UAV," IEEE/ASME Transactions on Mechatronics, Vol.19, No.2, pp.606-614, April 2014.
[4] M. Tanaka, Y. J. Chen, K. Tanaka and H. O. Wang, "A Simple Passive Attitude Stabilizer for Palm-Size Aerial Vehicles," IEEE/ASME Transactions on Mechatronics, Vol.21, No.1, pp.591-597, Feb. 2016.
[5] F. Tauro, C. Pagano, P. Phamduy, S. Grimaldi and M. Porfiri, "Large-Scale Particle Image Velocimetry From an Unmanned Aerial Vehicle," IEEE/ASME Transactions on Mechatronics, Vol.20, No.6, pp.3269-3275, Dec. 2015.
[6] J. J. Potter, C. J. Adams and W. Singhose, "A Planar Experimental Remote-Controlled Helicopter With a Suspended Load," IEEE/ASME Transactions on Mechatronics, Vol.20, No.5, pp.2496-2503, Oct. 2015.
[7] H. J. Kim, M. Kim, H. Lim, C. Park, S. Yoon, D. Lee, H. Choi, G. Oh, J. Park and Y. Kim, "Fully Autonomous Vision-Based Net-Recovery Landing System for a Fixed-Wing UAV," IEEE/ASME Transactions on Mechatronics, Vol.18, No.4, pp.1320-1333, August 2013.
[8] K. Tanaka, H. Ohtake, M. Tanaka and H. O. Wang, "Wireless vision-based stabilization of indoor micro helicopter," IEEE/ASME Transactions on Mechatronics, Vol.17, No.3, pp.519-524, June 2012.
[9] C. Luo, X. Li, Y. Li and Q. Dai, "Biomimetic Design for Unmanned Aerial Vehicle Safe Landing in Hazardous Terrain," IEEE/ASME Transactions on Mechatronics, Vol.21, No.1, pp.531-541, Feb. 2016.
[10] N. K. Ure, G. Chowdhary, T. Toksoz, J. P. How, M. A. Vavrina and J. Vian, "An Automated Battery Management System to Enable Persistent Missions With Multiple Aerial Vehicles," IEEE/ASME Transactions on Mechatronics, Vol.20, No.1, pp.275-286, Feb. 2015.
[11] D. Lee, A. Franchi, H. I. Son, C. Ha, H. H. Bulthoff and P. R. Giordano, "Semiautonomous Haptic Teleoperation Control Architecture of Multiple Unmanned Aerial Vehicles," IEEE/ASME Transactions on Mechatronics, Vol.18, No.4, pp.1334-1345, August 2013.
[12] P. Freeman, R. Pandita, N. Srivastava and G. J. Balas, "A Model-Based and Data-Driven Fault Detection Performance for a Small UAV," IEEE/ASME Transactions on Mechatronics, Vol.18, No.4, pp.1300-1309, August 2013.
[13] R. Nukki, T. Lehtla, A. Kilk and T. Kangru, "Design of the exterior-rotor PM synchronous motor for an electric powered paraglider," 2015 56th International Scientific Conference on Power and Electrical Engineering of Riga Technical University (RTUCON), Riga & Cesis, Latvia, Oct. 2015, pp.1-4.
[14] D. E. Meyer, M. D. Villa, I. Salameh, E. Fraijo, R. Kastner, F. Kuester and C. Schurgers, "Rapid Design and Manufacturing of Task-Specific Autonomous Paragliders Using 3D Printing," 2016 IEEE Aerospace Conference, Big Sky, Montana, March 2016, pp.1-8.
[15] J. Eckert, D. Eckhoff and R. German, "A deterministic radio propagation model for inter-paraglider communication," 2014 11th Annual Conference on Wireless On-demand Network Systems and Services (WONS), Obergurgl, Austria, April 2014, pp.138-142.
[16] T. Huba, I. Pestun and M. Huba, "Learning by pleasure - powered paraglider and other UAVs control," 2011 14th International Conference on Interactive Collaborative Learning (ICL), Piestany, Slovakia, September 2011, pp.548-552.
[17] C. Toglia, M. Vendittelli and L. Lanari, "Path following for an autonomous paraglider," 49th IEEE Conference on Decision and Control, Atlanta, Georgia, Dec. 2010, pp.4869-4874.
[18] Y. Ochi, H. Kondo and M.Watanabe, "Linear dynamics and PID flight control of a powered paraglider," AIAA Guidance, Navigation, and Control Conference, Chicago, Illinois, August 2009, AIAA 2009-6318.
[19] J. Umenberger and A. H. Goktogan, "System identification and control of a small-scale paramotor," 2013 IEEE International Conference on Robotics and Automation (ICRA), Karlsruhe, Germany, May 2013, pp.2970-2976.
[20] G. Lai, Z. Liu, Y. Zhang, and C. L. P. Chen, "Adaptive Position/Attitude Tracking Control of Aerial Robot With Unknown Inertial Matrix Based on a New Robust Neural Identifier," IEEE Transactions on Neural Networks and Learning Systems, Vol.27, No.1, pp.18-31, Jan. 2016.
[21] D. Nodland, H. Zargarzadeh and S. Jagannathan, "Neural Network-Based Optimal Adaptive Output Feedback Control of a Helicopter UAV ," IEEE Transactions on Neural Networks and Learning Systems, Vol.24, No.7, pp.1061-1073, March 2013.
[22] J. Shin, H. J. Kim, Y. Kim and W. E. Dixon, "Autonomous Flight of the Rotorcraft-Based UAV Using RISE Feedback and NN Feedforward Terms," IEEE Transactions on Control Systems Technologies, Vol.20, No.5, pp.1392-1399, August 2011.
[23] T. M. Barrows, "Multibody Parafoil Model," 20th AIAA Aerodynamic Decelerator Systems Technology Conference and Seminar, Seattle, Washington, May 2009, AIAA 2009-2945.
[24] M. Tanaka, H. Kawai, K. Tanaka and H. O. Wang, "Development of an autonomous flying robot and its verification via flight control experiment," 2013 IEEE International Conference on Robotics and Automation, Karlsruhe, Germany, May 2013, pp.4439-4444.
[25] M. Tanaka, K. Tanaka and H. O. Wang, "Practical Model Construction and Stable Control of an Unmanned Aerial Vehicle wth a Parafoil Type Wing," IEEE Transactions on Systems, Man, and Cybernetics: Systems, accepted, DOI:10.1109/TSMC.2017.2707393.